PAPER

Toward Real-Time, Remote Observations of the Coastal Wind Resource Using High-Frequency Radar

AUTHOR
Anthony Kirincich
Woods Hole Oceanographic Institution

ABSTRACT

There is now a large installed base of high-frequency (HF) coastal ocean radars in the United States able to measure surface currents on an operational basis. However, these instruments also have the potential to provide estimates of the spatially variable surface wind field over distances ranging from 10 to 200 km offshore. This study investigates the ability of direction-finding HF radars to recover spatial maps of wind speed and direction from the dominant first-order region radar returns using empirical models. Observations of radar backscatter from the Martha's Vineyard Coastal Observatory HF radar system were compared to wind observations from an offshore tower, finding significant correlations between wind speed and the backscatter power for a range of angles between the wind and radar loop directions. Models for the directional spreading of wind waves were analyzed in comparison to data-based results, finding potentially significant differences between the model and data-based spreading relationships. Using empirical fits, radar-based estimates of wind speed and direction at the location of the *in situ* wind sensor had error rates of 2 m/s and 60°, which decreased with hourly averaging. Attempts to extrapolate the results to the larger domain illustrated that spatially dependent transfer functions for wind speed and direction appear possible for large coastal ocean domains based on a small number of temporary, or potentially mobile, *in situ* wind sensors.
Keywords: remote sensing, HF radar, surface winds, calibration and validation

Introduction

High-frequency (HF) coastal ocean radar systems have proven to be highly effective at measuring surface currents on an operational basis. However, these instruments also have the potential to provide estimates of the spatially variable surface wind and wave fields over distances ranging from 10 to 200 km offshore. Knowledge of the spatial and temporal variability of the wind, wave, and current field is important in site assessment, performance prediction, and the operation of offshore wind and/or hydrokinetic power installations. Because of its ability to sample a large offshore region with minimal infrastructure and cost, land-based HF radar technology may be a practical way to obtain spatially resolved maps of the large-scale surface wind and wave fields.

Much of the progress on direct estimates of winds and waves via HF radars has been done using phased array (PA) systems (Wyatt et al., 2011). Wave extractions using these systems invert a low signal-to-noise ratio (SNR) portion of the returning signal for the wave field and, therefore, the wind field, through application of a wind wave model. However, the results are generally noisy and need to be integrated over periods of hour(s) as well as have reduced ranges relative to the full range of the radar (Green & Wyatt, 2006; Wyatt, 2000; Wyatt et al., 2011). Direct extractions of the spatially variable wind and wave fields have not been successfully demonstrated for direction-finding (DF) systems because of the more complex nature of the received backscatter signal (Lipa & Nyden, 2005).

However, recent work by Shen et al. (2012) using PA systems has shown that the primary part of the radar backscatter signal, called the "first-order" region, can be used to empirically relate the received radar power to the wind speed present with some success. Coupling this development to existing methods to derive wind direction from the difference of the two peaks in the first-order regions suggests that a simplified, direct path to remote observations of the wind resource for both the full domain of the radar and for short (15 min) averaging periods is possible. Such an approach circumvents the difficulties of using DF systems for wind and wave detection and thus could be applied equally to both PA and DF systems.

This study investigates the feasibility of using empirically determined transfer functions to predict the real-time spatial structure of the wind resource using DF systems. DF systems are more common in U.S. coastal waters, and thus, a method to utilize the first-order region to observe the temporally and spatially variable wind resource could be applied to a large base of operational systems with minimal capital expense. The proposed methods will be explored utilizing a new system of DF radars operated by the Woods Hole Oceanographic Institution (WHOI) along the southern New England shelf (Figure 1). This system of three medium-range SeaSonde HF radars is capable of observing the ocean environment at ranges of up to 50 km and with spatial resolutions as high as 400 m. A recent expansion of the WHOI system provides detailed observations within an area of interest for wind power development in the south of the islands as well as the New England Marine Renewable Energy Center's (MREC) Northeast Offshore Renewable Energy Innovation Zone (NOREIZ). Below, the HF radar backscatter signal and its relationship to surface winds are described first along with recent methods to extract wave and wind parameters, before details about the Martha's Vineyard Coastal Observatory (MVCO) radar system and wind data used are given. Next, comparisons of HF radar backscatter power observations from the location of an offshore tower measuring *in situ* winds are used to test existing models of the directional spreading of surface waves and compute HF radar-based wind direction and wind speeds at the location of the tower. These local results are then expanded to the high-resolution domain by assuming that real-time surface winds might vary spatially but are likely to be spatially uniform in the mean. A discussion of the results and future directions concludes this work.

FIGURE 1

The spatial extent of observations present in the new, expanded coverage area of the MVCO HF radar system, located south and west of the Islands of Martha's Vineyard (top) and Nantucket (right), respectively. Surface currents, in cm/s, are shown in the domain along with (black circles) the locations of the radar stations and the offshore tower and (red circle) the MVCO bottom-mounted node acoustic Doppler current profiler. The black box denotes the area of high-resolution coverage focused on deriving wind observations. (Color versions of figures are available online at http://www.ingentaconnect.com/content/mts/mtsj/2013/00000047/00000004.)

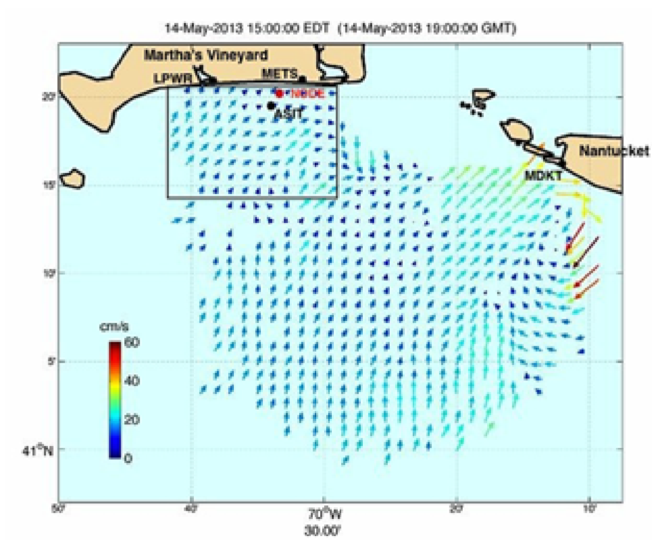

Background

The largest contribution to the backscattered power (the "first order" return) of a typical coastal radar system is scattering from surface waves whose wavelength is half the wavelength of the radar (Lipa & Barrick, 1983, 1986). These are known as "Bragg resonant waves," in analogy to scattering from a crystal or a diffraction grating. In the absence of a current, this coherent backscatter produces two peaks in the power spectrum of the radar return at +/− the phase speed of the Bragg wave (Figure 2), near 3 m/s for the 25-MHz systems utilized here. Advection of these waves by a current produces a Doppler shift in the location of the first-order peaks, and this observed displacement in speed can be used to infer the component of the current along the radar bearing. Returns from the same patch of water using two spatially separated radars enable estimation of the vector current. The Bragg peaks are flanked by a weaker "second-order" continuum due to double scattering from two freely propagating waves as well as scattering from nonlinearly bound waves (Barrick & Weber, 1977). This continuum contains contributions from all ocean wave components longer than the Bragg waves. Thus, the second-order part of the power spectrum can, potentially, be inverted to estimate the frequency-direction spectrum of the longer waves.

HF radars can be broadly grouped into two classes: DF and PA systems. PA systems utilize arrays of spatially separated antennas to form narrow directional beams by a spatial Fourier transform across the array. In this manner, PA systems are able to isolate the direction of arrival of incoming signals before computation of the

FIGURE 2

Sample backscatter power spectra for a 25-MHz Seasonde-type DF radar system. The peak energy near the "Bragg wave" Doppler shift (vertical red lines) is visible as is the second-order energy due to wave effects. The difference in power between the positive and negative Doppler velocities is used to estimate wind direction.

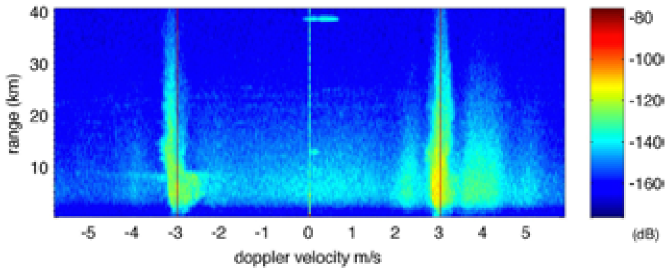

backscatter power spectra (i.e., Figure 2), achieving individual power spectra for each azimuthal bearing of the radar. DF radar systems utilize a compact array of three, colocated antennas and require the application of DF algorithms on the measured backscatter power spectra to determine the azimuthal bearing of each received signal. The abilities of these algorithms to resolve the bearing of signals in the first-order region are well documented (Kohut & Glenn, 2003; Lipa & Barrick 1983, 1986; Lipa et al., 2006; Paduan et al., 1999) and generally require carefully calibrated antennas. Most technical approaches to estimate wind speed and direction have utilized the wave information inferred from the radar return (Wyatt et al., 2011). This is preferable to, for example, trying to relate winds to the measured currents as that relationship is complicated in the coastal ocean and because short waves respond much more rapidly to the wind (Figure 3). The radars used in this study operate around 25 MHz, giving a Bragg wavelength of roughly 6 m (or a period of 2 s). It is generally assumed that waves this small follow the wind closely. The spectral level of waves in this "equilibrium range" of the surface wave spectrum is wind speed dependent (Terray et al., 1996). In typical coastal environments, these waves include and can be longer than the Bragg waves. Hence, if the HF part of the long wave spectrum can be recovered from the second-order portion of the backscatter signal, the wind speed can be estimated directly.

FIGURE 3

Relationships of the (clockwise from lower left) near-surface currents, significant wave height, and wind waves in the equilibrium range to the wind speed during an hour of increasing wind speed, as observed by Terray et al. (1996). The bottom right panel shows time series of all three, using matching colors/symbols, as well as the wind stress itself (blue squares). For these fetch-limited conditions, the equilibrium range wave level tracks the wind closely, and the significant wave height waves (here, 2- to 3-s waves) do moderately well, while the currents have no coherence to the wind speed. (Figure courtesy of E. Terray.)

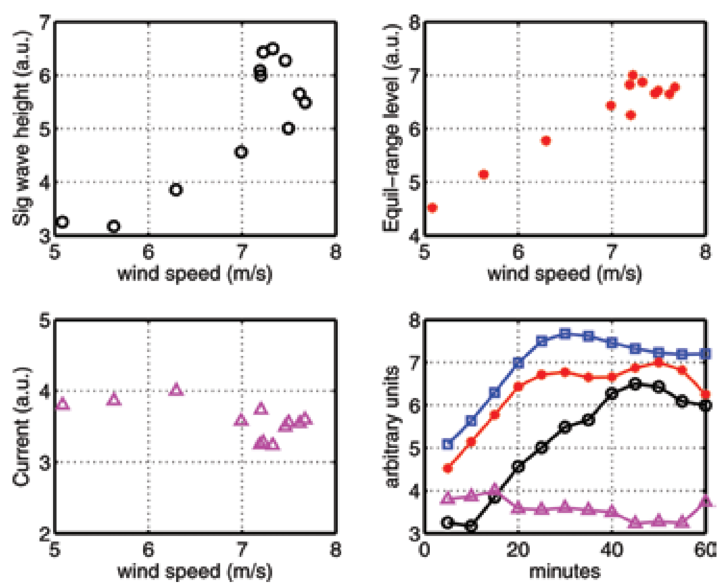

Recovering the long wave spectrum using inversions of the second-order portion of the radar backscatter has been done using PA-type radar systems (Green & Wyatt, 2006; Heron, 2004; Heron & Rose, 1986; Hisaki, 2004; Lipa, 1978; Wyatt, 2000; Wyatt et al., 2003, 1997). These techniques have been able to estimate both the wave and wind fields at angular resolutions similar to those of the current measurements, but with reduced ranges. Accurate methods for DF signals in the second-order region of the backscatter power of a DF system have not been developed. At the present time, the Seasonde DF system provides a single, coarse estimate of the average significant wave height, dominant wave period, and wind direction over a radial range circle close to the radar on an operational basis. These estimates are based on a least-squares fit of the Pierson and Moskowitz (1964) model for the ocean wave spectrum, placed in a Fourier series representation of the theoretical second-order portion radar spectrum integrated along a range circle, to the observed radar spectrum (Lipa & Nyden, 2005).

A Direct Path to Wind Speed and Direction

However, a more direct path to estimating wind speed and direction using both types of HF radar systems exists. As recently described by Shen et al. (2012), the backscatter power observed within the first-order or Bragg region is a direct function of the wind speed. Following their notation, the power of the incoming or receding Bragg wave energy is dependent on the directional spectrum of the Bragg wave field (G), the energy spectrum of the Bragg waves (E), and an unknown constant (κ).

$$P_1(+f_B) = \kappa\, E(f_B) G(\pi + \Phi_o - \theta_B) \quad (1)$$

$$P_1(-f_B) = \kappa\, E(f_B) G(\Phi_o - \theta_B) \quad (2)$$

where Φ_o and θ_B are the wind and radar bearings for the incoming, $P_1(+f_B)$, and receding, $P_1(-f_B)$, Bragg waves. A number of functional forms of G have been proposed (Paduan et al., 1999; Shen et al., 2012), including trigonometric functions such as cosines or hyperbolic secants raised to the second or fourth power (Figure 4). These directional dependences for G are used to map the direction of coastal winds with HF radars by comparing the ratio of the approaching and receding Bragg wave energy peaks to the wind-wave directional spreading model to estimate the mean wind direction (Paduan et al., 1999; Shen et al., 2012). The Bragg wave energy, E, should vary with the wind speed for a broad range of the wind conditions present in the coastal ocean (Shen et al., 2012). The Bragg waves themselves are generally within the equilibrium range of the wave energy spectrum for wind speeds of 2–10 m/s (4–20 knots) for 25-MHz systems (i.e., Bragg waves of 2 s) and 5–15 m/s (10–30 knots) for 5- to 7-MHz systems (i.e., Bragg waves of 4.5 s). Thus, the Bragg waves from most radars should track the wind speed and direction well over a frequency-dependent range of wind speeds. The one caveat to this approach is that the magnitude of the backscatter power of the two Bragg peaks is also dependent on the unknown constant, κ. This constant is dependent on the internal components of the radar system, the location within the domain, as well as potentially related to wind direction and speed itself. Additionally, κ has the potential to be slowly varying in time due to internal changes (component wear, etc.) in the radar systems. Thus, κ cannot be theoretically determined and must be field calibrated (Paduan et al., 1999).

Despite this, the advantages of using the Bragg region to determine the wind speed and direction over full inversions of the second-order regions are numerous. The higher SNRs in the Bragg region mean that estimates are possible over the full range of the radar. Estimates are possible over shorter-time (5–15 min) data samples opening up a greater potential for real-time operational status. If the unknown constants are time invariant, or at least slowly varying, a long-term calibration will be able to correctly predict the wind in rapidly changing conditions. Finally, use of the Bragg region allows these methods to be easily applied to DF systems as well as PA radar systems. As DF systems dominate U.S. observational assets, this would open up vast tracks of the coastal ocean to remote, low cost, wind resource characterizations. The recent work of Shen et al. applied trained neural network techniques to invert for the wind speed and direction from the Bragg peaks of a PA radar system, using a sophisticated model that included variability due to fetch, or wave age, and wave spreading. Their results for similar frequencies to that used here generally found root-mean-square (RMS) wind speed errors of 2–3 m/s and directional errors of 20°–30° (Shen et al., 2012) for hourly averaged data.

The present study takes a more basic approach and focuses on the potential use of *in situ* wind observations to directly calibrate the unknown system constants throughout

FIGURE 4

Models of wave directional spreading about the mean wind direction for an arbitrary wind direction and magnitude. Shown are the sech$^2(\theta)$ model (in black) suggested by Donelan et al. (1985) and Shen et al. (2012) and the smaller cos$^4(\theta/2)$ model (in gray) suggested by Longuet-Higgins et al. (1963) and Steward and Barnum (1975).

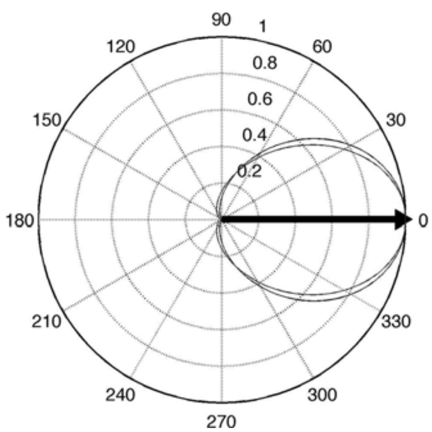

the domain observed by a DF HF radar, thereby recovering wind speed estimates over a wide spatial area using a single *in situ* wind sensor. A central assumption of this work is that, in the mean, the winds measured at one location will be representative of winds present over a larger domain. This assumption allows for temporally variable spatial structure (i.e., transient fronts or jets) to exist but requires the mean spatial structure to be homogenous. Using this assumption to build relationships between the power and wind speed at all locations would allow predictions of real-time spatial structure in the wind resource. Additionally, noise in the observed radar backscatter is likely to be the largest source of error in a regression between the backscatter power and wind speed, far above the variability due to fetch or wave age considered by Shen et al. (2012). With this second assumption in mind, the present work focuses solely on examining simple regressions between the backscatter power and wind speed with the goal of answering the following questions: How large of a domain can be reasonably calibrated from a single *in situ* wind sensor? Can a short *in situ* data set achieve reasonable results? How well do models for the directional spreading of wind waves (e.g., Lipa & Nyden, 2005; Paduan et al., 1999) compare to data-based directional spreading relationships?

Observations

Observations collected by the 25-MHz coastal radar system installed by WHOI at the MVCO south of the islands of Martha's Vineyard and Nantucket, Massachusetts (Figure 1), will be used in this study. As described in detail by Kirincich et al. (2012), the system is composed of three CODAR Ocean Sensors SeaSonde instruments that were deployed to realize the highest spatial resolution possible, ~400 m, as well as to resolve currents just offshore, ~700 m, of the coast within a 300-km^2 domain directly south of Martha's Vineyard (sites Long Point Wildlife Refuge [LPWR], METS, and ASIT in Figure 1). A recent move of one of the sensors from the MVCO offshore tower (ASIT, Figure 1) to Nantucket (MDKT, Figure 1) created a second overlapping 4000-km^2 grid covering most of the southern New England shelf with 1.5-km resolution. This larger domain encompasses the majority of the Massachusetts's area of interest for wind power development and MREC's NOREIZ.

For CODAR-type systems, DF algorithms (Barrick & Lipa, 1997) are used to determine the bearing of signals detected within the first-order region and average the resulting radials into 5°-wide azimuthal bins. For the WHOI system, the response pattern of each antenna system has been routinely measured and carefully calibrated (approximately every 6 months) using analyses of the spatial structure of observed tidal ellipses to iteratively minimize time-invariant bearing-related errors. Due to new methods developed by Kirincich et al. (2012), the WHOI high-resolution system has been found to have real-time accuracies of 4–5 cm/s, defined as RMS differences from *in situ* acoustic Doppler current profiler measurements.

While the system has been operating since November 2010, radar observations collected over a 10-day period in August 2011 will be utilized for the present work to determine what is possible with a limited amount of *in situ* calibration data and typical summertime conditions having variable winds. For the time period in question, the radar backscatter from all sites, available at independent 15-min sample periods, was reprocessed using the MUSIC DF algorithm to record the range, bearing, and calculated signal power for every first-order solution within both the incoming and receding Bragg regions.

Wind observations from MVCO's offshore tower (ASIT in Figure 1) will be used for *in situ* ground truthing, as all three systems have overlapping coverage of the tower location. A three-axis sonic anemometer on the tower collected burst-averaged estimates of wind speed and direction every 20 min at a height of 18 m above sea level. The tower wind measurements were converted to standard 10-m height observations following Large and Pond (1981) assuming neutral stability and interpolated to the 15-min sample periods of the radars.

Results

Comparisons at the Location of the Wind Observations

From each of the three radar sites, the backscatter power from incoming and receding Bragg returns, determined via DF to originate from a 1-km-diameter circle around the location of the MVCO offshore tower (ASIT, Figure 1), were spatially grouped for each 15-min sampling period. Within each group, a number of statistical products were created, including the mean power, the median power, the maximum power, and 90th percentile of the backscatter power. All were evaluated for their correspondence to the wind (not shown), and the maximum observed power level was found to be most responsive to the wind. Thus, the maximum power level is used exclusively below to estimate the wind direction and wind speed from the radar returns.

The time series of maximum power were utilized to estimate the Bragg ratios, the difference in power of the backscatter from the incoming and receding waves (Paduan et al., 1999). For each radar, Bragg ratios were compiled by their wind direction relative to the radar, that is, the angle between the wind direction and the bearing to the location of the wind sensor from the radar, to document the observed dependence of the Bragg ratio on the orientation of the relative wind direction (Figure 5). The observed Bragg ratios generally decreased from a bin averaged maximum value near 15 dB for all radars but had different functional forms for the data from each radar site. While the data for ASIT and LPWR were generally positive for all possible difference angles, ratios for ASIT decreased more slowly. At METS, the Bragg ratios became negative for angles less than about ±100°.

These results were compared to models for the directional spreading of wind waves suggested by Longuet-Higgins et al. (1963) and Donelan et al. (1985) and used by Steward and Barnum (1975), Paduan et al. (1997), and Shen et al. (2012) to test the correspondence of the models of directional spreading to Bragg power observations. For the comparisons shown in Figure 5, the model distributions were normalized to the peak values of the observed, bin averaged, Bragg ratios found at angular differences of 0°. This observed peak value for the "downwind" Bragg ratios was significantly less than the 24 dB determined by Long and Trima (1973) using sky-wave radar measurements. Additionally, even when the roll-off of the model Bragg ratio with angle did appear to agree with the observations (e.g., positive angles at METS), the differences between the models used were small relative to the scatter of the observations (Figure 5).

The discrepancies between observations and the spreading models shown in Figure 5 have significant effects on time series of wind direction estimated using radar observations and the spreading models. To illustrate this, radar-based estimates of wind direction were estimated using the Bragg ratios from all radars following the methods described by Paduan et al. (1999), assuming the $G(\theta) = \cos^2(\theta/2)$ model of directional spreading and normalizing by the observed mean downwind maximum value of 15 dB. A second estimate of the radar-derived wind direction used a data-based lookup table of the Bragg ratio dependence on relative wind direction at each site, formed using a smoothed version of the bin averaged, observed Bragg ratios (Figure 5, red lines). Using these lookup tables for all sites in place of the spreading models, the two possible difference angles for each site, due to directional ambiguity of the Bragg ratio estimates (Paduan et al., 1999), were estimated and combined as follows to estimate the wind direction. The mean direction and standard deviation of all possible combinations (up to six) of these angles were computed, and the mean direction with the smallest standard deviation was chosen to be most representative of the true wind direction present.

As shown in Figure 6, the data-based estimate of wind direction had reduced scatter relative to the results possible using the theoretical spreading model. RMS difference values for the estimated wind direction during the study period decreased from 76° for the model-based winds to 62° for the data-based winds. However, for both, the wind direction estimates performed best when winds were generally from the south or onshore but diverged more significantly from the measured wind direction for along-shelf winds, particularly for the time period near August 5.

FIGURE 5

Individual estimates (gray) and bin averages (black, with standard error) of the Bragg ratios against the difference of the wind bearing and the radar bearing, the direction to the *in situ* wind sensor from each of the radar sites (i.e., 0 is for winds from the radar to the wind sensor and ±180 is for winds from the sensor to the radar). The directional spreading models proposed by Donelan et al. (1985) and Longuet-Higgins et al. (1963) are shown as dashed and solid lines for comparison. A smoothed version of the bin-averaged results (red) is used in the text to compute the data-based directional spreading.

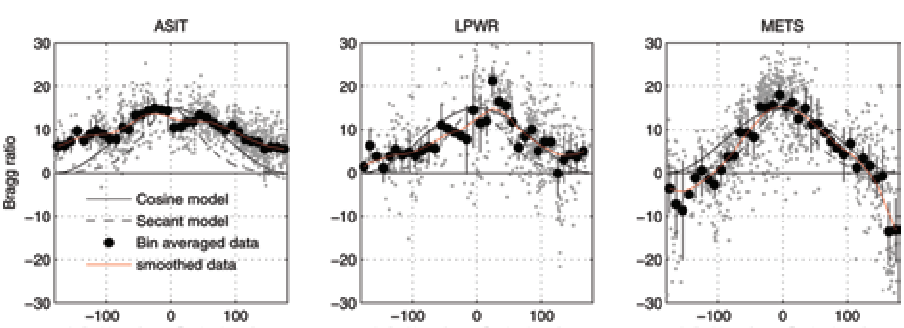

FIGURE 6

Time series of predicted (circles) and observed (black line) wind direction using the cosine model (upper panel) and site-specific data-based observations (lower panel) to estimate wind direction from the Bragg ratios observed at all sites.

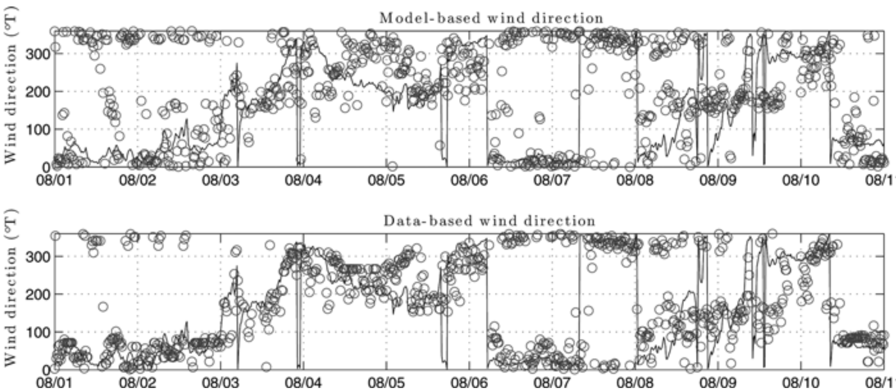

Additionally, it should be noted that the results shown are for independent 15-min samples of the radar backscatter. This high temporal resolution sampling was found to cause a significant fraction of the scatter seen in individual estimates of the Bragg ratios and represents a source of noise to the estimated wind direction and, therefore, the vector winds. Longer sample intervals (hourly) were found to have reduced errors relative to the results shown. Additional efforts that raise the lower bound for Bragg ratios allowed by the calculation were found to further reduce RMS differences but also reduced the amount of viable results.

Continuing to focus on the results from the location of the tower winds, the raw relationship between observed backscatter power and wind speed was examined next. For the data from each site, times when the observed winds were ±15° from the bearing line between the radar location and the tower were first isolated. These comparisons should have the strongest signal from the wind with minimal effects of directional spreading on the observed power levels. As the averaging circle for the ASIT site, located on the tower, includes radials from all directions, winds along the bearing line between the tower and METS were used for this site. Comparisons using ASIT data from the averaging circle are consistent with those from METS or LPWR, despite its colocation with the wind sensor itself. Because the maximum power results are used here, the dominant response is likely to be from the downwind radials, despite the variety of radial directions included in the averaging circle.

In the top panels of Figure 7, power versus wind speed results for winds within ±15° of the bearing line between the site and the wind sensor are shown for incoming (positive, onshore winds) and outgoing (negative, offshore winds) Bragg waves for all three radar sites. Bin averages, with standard errors, and best-fit linear slopes are also shown, calculated for wind speeds between 2 and 10 m/s, the theoretical range of wind speeds when the Bragg wave, having a 6-m wavelength, is within the equilibrium range. At all sites, the wind speed-power relationships had greater slopes, that is, a greater dynamic range, when winds were offshore. Slopes for the relationship between onshore winds and signal powers were more moderate, but significant scatter existed in all the relationships shown.

The middle and bottom panels of Figure 7 describe the correspondence between the wind speed and radar power for conditions when the angle between the wind and radar bearings ranges from 15° to 45° (middle panels) and 45° to 90° (lower panels). In general, the best-fit slopes and correlation coefficients between the wind speed and backscatter power for the 15°–45° comparisons were similar to that found for downwind conditions. This occurred despite the potential variations shown in the theoretical spreading model over the same range of angles (Figure 4). Correlation coefficients between power and wind speed degraded more significantly when winds were 45°–90° from the radar downwind direction but were reasonable for some of the radar site results (i.e., LPWR or METS for negative wind speeds).

Thus, perhaps due to the inherent noise of the radar systems in generating scatter or the true functional form of wind wave spreading, the relationship between the wind speed and backscatter power over a wide range of relative wind directions can be represented, for each radar and location, by a single estimate of the regression between the power and wind speed. These similarities effectively open a greater range of wind directions where the wind speed can be empirically predicted from the signal power using the linear fits shown.

Testing this simple predictive model, for each time when a wind direction solution existed and when the estimated direction was within 75° of the bearing line to a radar site, the wind speeds were estimated from the

FIGURE 7

Comparisons of wind speed at the offshore tower versus average power from a 0.5-radius circle around the tower as observed from (left panels) ASIT, (middle panels) LPWR, and (right panels) METS during times when the observed wind was (top panels) ±15°, (middle panels) 15°–45°, and (bottom panels) 45°–90° from the bearing line between the wind sensor and the radar location. Results are shown for incoming (onshore winds, positive wind speeds) and outgoing (offshore winds, negative wind speeds) waves. Locations for the radar sites are shown in Figure 1, and best-fit linear slopes and correlation coefficients are shown for each comparison.

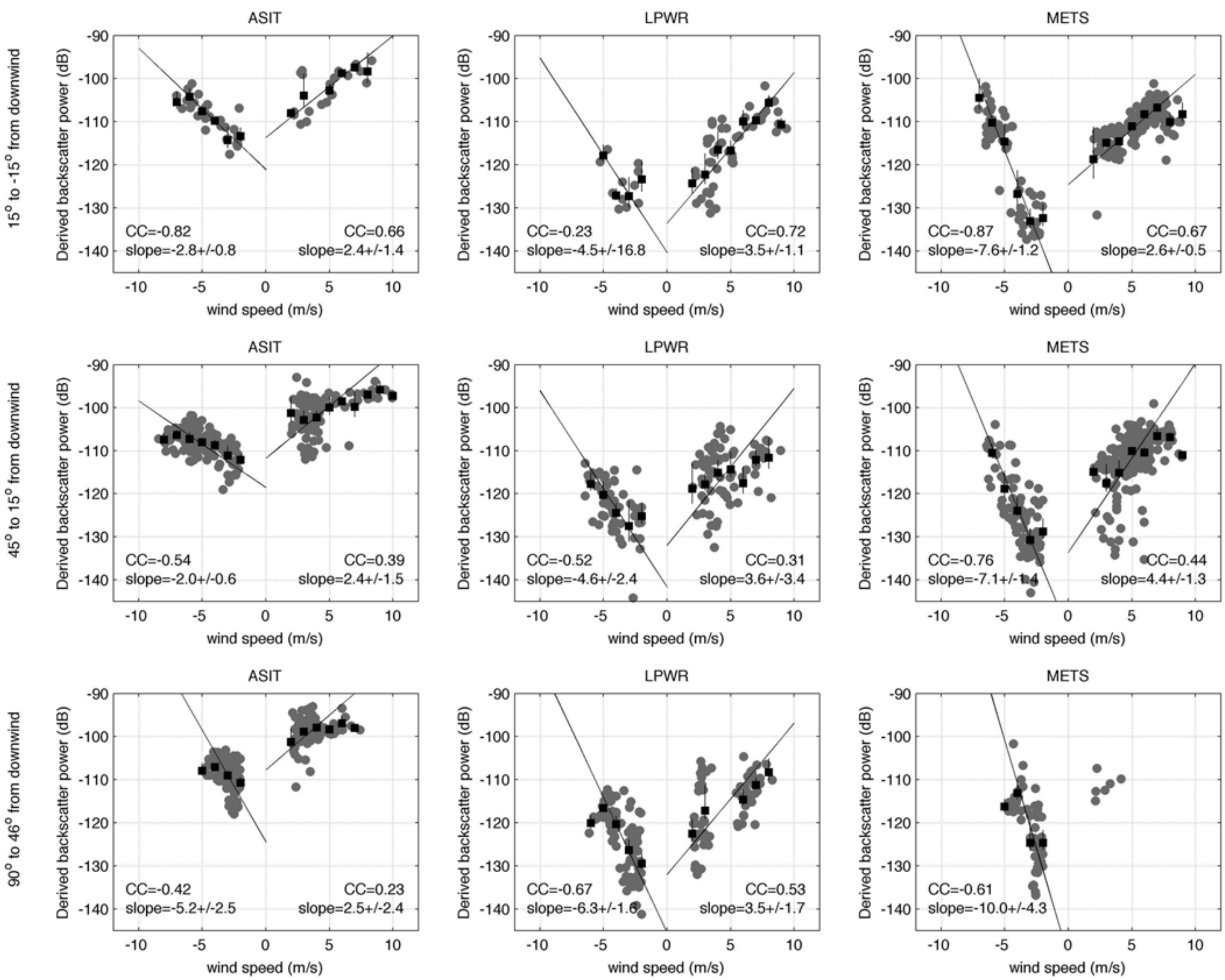

radar power and the linear relationships shown in Figure 7. Results from multiple sites for the same times were averaged to form a single estimate of HF radar-based wind speed. The expansion to ±75° was found to be the widest angular range possible without decreasing the performance of the wind speed results. With or without this expansion, predictions of wind speed based on the radar power were quite variable (Figure 8), likely due to the scatter of radar power about the linear fits shown in Figure 7. However, the radar-based estimates were significantly correlated to the observed wind speed (CC = 0.56) with RMS differences of 1.8 m/s and a regression slope of <1. Likely to the small amount of data present from winds greater than 8 m/s, the radar-estimated wind speed under predicted observed winds at these speeds. As shown in the time series comparison in Figure 9, this was predominantly due to poor performance during the wind event on August 7.

Extrapolation of the Method to a Larger Area

The methods described above to utilize the *in situ* wind sensor to

FIGURE 8

Observed wind speed versus the radar-based prediction for wind speed at the location of the *in situ* wind sensor.

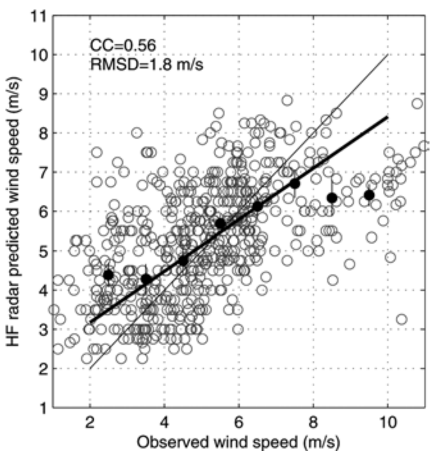

calibrate radar-based wind speed and direction estimates were extended to a 1 km × 1 km resolution grid within the MVCO high-resolution domain (Figure 1, black box) to understand both how representative the *in situ* winds were of the area and how well a single sensor could be used to calibrate radar-based estimates over a broader area. As described earlier, using the observations of a single *in situ* wind sensor to calibrate a broader spatial area requires the assumption that the measured *in situ* winds are, at least in the mean, representative of winds everywhere in domain to the accuracy of the radar-based wind estimates. It is important to note that this assumption does not preclude the existence of a spatially variable wind field; it simply requires that the spatial structures present be transient and that no permanent features of the wind field exist.

Thus, the tower-based *in situ* wind observations were used to estimate data-based wind direction and wind speed transfer functions for all locations within the radar domain. These estimates were done exactly as described above, in that the measured winds were assumed to originate from the grid point in question, and the backscatter power calculations were computed for winds directed along the bearing line between the radars and the grid point in question as well as winds at higher relative wind directions. Thus, the wind speed regressions and wind direction lookup tables for each individual grid point differ from those shown in Figures 6 and 7 as the bearing lines to the grid point from radar stations varied with the grid point, and the wind observations were always rotated into the coordinate system of the radar bearing line.

Two metrics that help understand the quality of these results and their usefulness were the correlation coefficients and RMS differences between the radar-based wind speed estimates and the *in situ* wind sensor (Figure 10, top panels). In general, the highest correlations were in the area around the *in situ* observations with decreasing correlations with distance away from the tower. By 4–6 km away from the site, correlations generally dropped below 0.5. Without more information, it is not possible to say for certain whether correlation patterns were due to variability in the wind field or noise in the radar observations. RMS differences show a similar pattern, with lower errors (<2 m/s) observed in the area adjacent to the tower and inshore of the 20-m isobath but increasing errors offshore. Regression slopes

FIGURE 10

Spatial maps of (top) correlation coefficients, (middle) RMS differences, and (bottom) linear regressions slopes between the observed wind speed, assumed representative of winds throughout the domain, and the radar-estimated wind speed present at each 1-km-spaced grid point.

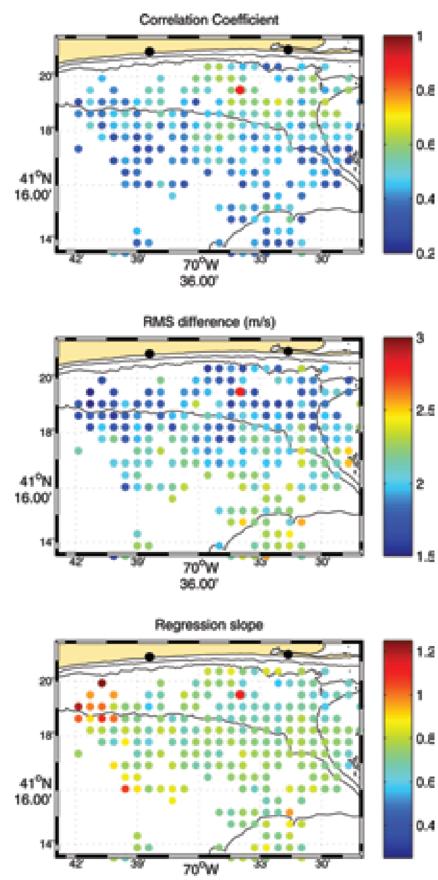

FIGURE 9

Time series of predicted (circles) and observed (black line) wind speed at the location of the *in situ* wind sensor.

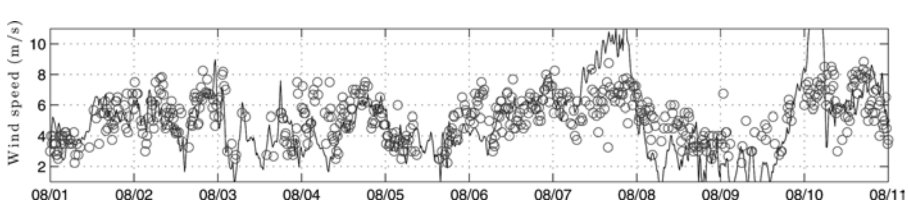

between the resulting radar-based wind speeds and the *in situ* observations were generally less than one throughout most of the domain (Figure 10, bottom panel). Analysis of the individual results at all grid points (not shown here) suggested that these differences were due mostly to a poor representation of the high wind speeds found on August 7. Finally, there is a small but notable offshore gradient to these estimated metrics, indicating that fetch limitations may play a more prominent role in setting the wind speed versus power relationships during times of offshore winds.

For those areas where the comparisons between the *in situ* wind sensor and the radar-based wind speed estimates appear viable, defined here as statistically significant correlation coefficients greater than 0.5, an example of the radar-estimated, instantaneous winds at 4:45 GMT on August 6, 2011, gives an idea of the size of coverage area potentially available for real-time winds from the radar system using a single calibration sensor. Shown in Figure 11, onshore winds are available from a broad area, including ~15 km along-shelf and ~10 km across-shelf, and suggest some veering of the winds with along- and across-shelf locations, particularly over the tidal shoals found to the east of the *in situ* wind sensor.

Discussion and Conclusions

The purpose of this paper was to explore the potential use of DF coastal radar systems for making observations of surface wind speed and direction over large areas of the coastal ocean. HF radar-based observations of the surface wind resource using the Bragg region of the radar returns, as opposed to the more commonly studied

FIGURE 11

Radar-estimated wind vector (speed and direction) at 4:45 AM on August 6, 2011 (GMT), for all grid points with significant correlations of estimated winds and the *in situ* wind sensor between August 1 and 11.

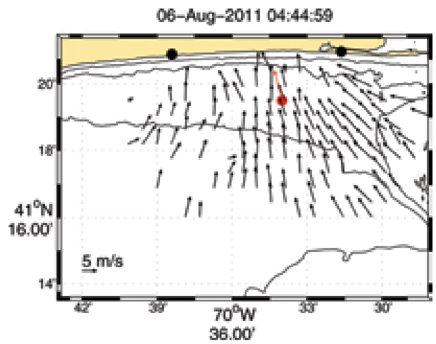

second-order region, offer a potential pathway for remote, real-time sensing of the wind resource on scales of 15 min and 1–2 km ranging up to 50 km offshore with medium-range radar frequencies. Further offshore ranges would be possible with lower frequencies, but with a frequency-dependent wind speed range (2–10 m/s for 25 MHz and 5–15 m/s for 5–7 MHz). The key to widespread use of this portion of the backscattered signal for winds is the ability to estimate radar-dependent constants that are both instrument and location specific. As shown here, building empirical relationships out from areas of *in situ* wind sensors is a potentially useful way to estimate this unknown factor and can be utilized on DF radar systems as well as PA systems. Additional techniques such as the neural networks training model used by Shen et al. (2012) may be useful in expanding the comparisons of *in situ* wind sensors to other areas. However, the sources of the scatter or noise in the estimates must also be understood and mitigated to increase the utility of the method.

Based on the results shown above, using radar frequencies near 25 MHz, real-time maps of the wind resource would have speed errors of ~2 m/s and directional errors of up to 60° for 15-min averages. While these results show some promise, these accuracy levels might be larger than what would be required by operators and resource managers. Thus, additional work is needed to assess whether error levels can be reduced further by improving the ability of the wind direction estimates while maintaining temporal and spatial independence; resolving the role of noise, including wave fetch, on wind speed regressions; and documenting the variability of the constants with time and among similar systems.

Briefly addressing the first two of these topics, additional work using the MVCO data set (not shown here) suggested that noise in the backscatter power estimates contributes significantly to the scatter shown in the directional mapping (Figure 6). As evidence of this, estimates of wind direction using hourly averaged results yielded RMS differences from observations that were similar to that found by Shen et al. (2012). Given the large scatter observed using the Bragg ratios shown in Figure 5, spectral estimates with improved noise characteristics, that is, shorter fast Fourier transforms with more overlap and averaging, might improve the directional estimates within a 15-min window enough to not require longer-term averaging or smoothing.

Additionally, despite the scatter shown in Figure 7, the predicted wind speed was consistently equal to the observations on numerous occasions. These periods appeared at all levels of wind speed and direction, suggesting that the factors driving instances of large differences were not simply due to random noise or a breakdown of the simple wind-wave relationships assumed in the linear transfer functions but due to potentially nonrandom radar-related noise. This is particularly true at higher wind speeds where the estimated wind speeds under predicted the winds present.

While some of these issues could be resolved with the use of multiple radar frequencies having varying wind speeds of optimal response, the role of fetch, or wave age, in potentially causing a portion of the errors seen here is an important topic that needs further research. Given the different relationships shown in Figure 7 for onshore winds, with potentially unlimited fetch, and offshore winds with a fetch of 4–7 km, wave age is obviously an important aspect of the wind speed/radar power relationship. Additionally, the scatter of observed power was generally larger for onshore directed, or positive, winds. Thus, a focused effort to include wave age, perhaps via a multiple regression analysis, might be able to reduce the uncertainty of the wind speed estimates further but would likely require longer calibration data sets as well as be dependent on a real-time estimate of the wave spectrum made within the radar domain.

Thus, the topics and issues described above suggest a path forward to improve HF radar-based estimates of the coastal wind resource and bring them to an operational status. Additional efforts at noise reduction are likely to further decrease errors, both in wind speed and wind direction, as hourly averaged power estimates were able to reduce RMS differences to ~1.5 m/s and 20°–30° with the MVCO data set. Achieving these levels at higher temporal resolutions appears possible but is likely a function of the types of products that wind resource users and managers are interested in obtaining, and thus, some feedback is necessary as work on cost-effective ways to characterize the coastal wind resource progresses.

Finally, this work has documented that calibrations from an *in situ* sensor appear to have a limited spatial range. Thus, while the deployment of buoy-based wind sensors in key areas is likely to be an important component of a directed field campaign, finer scale calibration data are necessary as well. However, the results also showed that the calibrations do not require a large amount of data. This suggests that satellite-based or mobile autonomous surface sensors should be able to calibrate a large spatial area with limited resources. Satellite-based synthetic aperture radar wind speed estimates are notable for their high spatial resolution (~100 m/s) and similar error rates to those described here (~2 m/s) but have poor temporal resolution (~30 passes of a given area such as the Mid-Atlantic Bight per year). Thus, these platforms are not able to provide real-time estimates of the wind resource or accurately estimate the climatology of the wind resource within a region of interest. However, the limited data might be well suited for calibrating the radar-based wind estimates, which could provide both the real-time and climatological wind resource information needed. Second, recent developments in mobile autonomous surface vehicles have shown that such units are capable of measuring *in situ* winds, waves, and currents along established survey grids over long time periods with minimal operational costs. A single 2- to 3-month deployment of a mobile surface vehicle could be used to calibrate an entire region of interest. Additional gains in accuracy and reliability will be a function of the types of information needed by the wind energy community.

Summary

Observations of radar backscatter from the MVCO's HF radar system were compared to wind observations from an offshore tower, finding significant correlations between wind speed and backscatter power, enabling radar-based estimates of wind speed and direction throughout a 10 km × 15 km area around the tower. The empirically determined transfer functions used to derive wind speed from the radar backscatter power were found to have RMS differences of up to 2 m/s and angular differences up to 60° for 15-min samples, due in part to times when winds were along-shelf and poorly resolved by all radar systems. The error levels were most likely due to noise in the radar-estimated power, as longer-term averages of the backscatter results produced higher-quality results. However, additional discrepancies due to the simple regressions of wind direction and speed used might have also played a role and are worthy of further study. If radar noise issues could be further mitigated, spatially dependent transfer functions for wind speed appear possible for large coastal ocean domains based on the data from targeted calibrations collected by mobile or satellite platforms.

Acknowledgment:

This work was supported by the New England Marine Renewable Energy Center (Subaward 12318) via funding from the Massachusetts Clean Energy Center.

Author:

Anthony Kirincich
Woods Hole Oceanographic Institution,
Woods Hole, MA 02543
Email: akirincich@whoi.edu

References

Barrick, D.E., & Lipa, B.J. 1997. Evolution of bearing determination on HF current mapping radars. Oceanography. 2(10):72-5.

Barrick, D.E., & Weber, B.L. 1977. On the nonlinear theory for gravity waves on the ocean's surface. Part 2. Interpretation and Applications. J Phys Oceanogr. 7:11-22. http://dx.doi.org/10.1175/1520-0485(1977)007<0011:OTNTFG>2.0.CO;2.

Donelan, M, Hamilton, J, & Hui, W. 1985. Directional spectra of wind-generated waves. Philos T R Soc S-A. 315:509-62.

Green, L.L., & Wyatt, L.R. 2006. Row-action inversion of the Barrick-Weber equations. J Atmos Ocean Tech. 23:501-10. http://dx.doi.org/10.1175/JTECH1854.1.

Heron, M.L. 2004. The effect of bimodal sea spectra on HF radar wind analysis. In: OCEANS'04. MTTS/IEEE TECHNO-OCEAN'04. IEEE Oceans. 1:537-41.

Heron, M.L., & Rose, R.J. 1986. On the application of HF ocean radar to the observation of temporal and spatial changes in wind direction. IEEE J Oceanic Eng. 11:210-8.

Hisaki, Y. 2004. Short-wave directional distribution for first-order Bragg echos of the HF ocean radars. J Atmos Ocean Tech. 21:105-21. http://dx.doi.org/10.1175/1520-0426(2004)021<0105:SDDFFB>2.0.CO;2.

Kirincich, A., de Paolo, T., & Terrill, E. 2012. Improving HF radar estimates of surface currents using signal quality metrics; with application to the MVCO high-resolution radar system. J Atmos Ocean Tech. 29:1377-90. http://dx.doi.org/10.1175/JTECH-D-11-00160.1.

Kohut, J.T., & Glenn, S.M. 2003. Improving HF radar surface current measurements with measured antenna beam patterns. J Atmos Ocean Tech. 20:1303-16. http://dx.doi.org/10.1175/1520-0426(2003)020<1303:IHRSCM>2.0.CO;2.

Large, W.G., & Pond, S. 1981. Open ocean momentum flux measurements in moderate to strong winds. J Phys Oceanogr. 11:324-36. http://dx.doi.org/10.1175/1520-0485(1981)011<0324:OOMFMI>2.0.CO;2.

Lipa, B.J. 1978. Inversion of second-order radar echoes from the sea. J Geophys Res. 83(C2):959-62. http://dx.doi.org/10.1029/JC083iC02p00959.

Lipa, B.J., & Barrick, D.E. 1983. Least-squares methods for the extraction of surface currents from CODAR crossed-loop data: Application at ARSLOE. IEEE J Oceanic Engr. OE-8:226-53. http://dx.doi.org/10.1109/JOE.1983.1145578.

Lipa, B.J., & Barrick, D.E. 1986. Extraction of sea state from HF radar sea echo: Mathematical theory and modeling. Radio Sci. 21:81-100. http://dx.doi.org/10.1029/RS021i001p00081.

Lipa, B.J., & Nyden, B. 2005. Directional wave information from the SeaSonde. IEEE J Oceanic Eng. 30(1):221-31. http://dx.doi.org/10.1109/JOE.2004.839929.

Lipa, B.J., Nyden, B., Ullman, D.S., & Terrill, E. 2006. Seasonde radial velocities: Derivation and internal consistency. IEEE J Oceanic Eng. 31(4):850-61. http://dx.doi.org/10.1109/JOE.2006.886104.

Long, A.E., & Trima, D.B. 1973. Mapping of North Atlantic winds by HF radar sea backscatter interpretation. IEEE T Antenn Propag. AP-21:680-85. http://dx.doi.org/10.1109/TAP.1973.1140557.

Longuet-Higgins, M.S., Cartwright, D.E., & Smith, N.D. 1963. Observations of the directional spectrum of sea waves using the motions of a floating buoy. In: Ocean Wave Spectra. Prentice-Hall: Englewood Cliffs, NJ. pp. 111-36.

Paduan, J., Delgado, R., Vesecky, J., Fernandez, Y., Daida, J., & Teague, C. 1999. Mapping coastal winds with HF Radar. In: Proceedings of the IEEE Sixth Working Conference on Current Measurement. pp. 28-32. IEEE: San Diego. http://dx.doi.org/10.1109/CCM.1999.755209.

Pierson, W.J., & Moskowitz, L. 1964. A proposed spectral form for fully developed wind seas based on similarity theory of S. A. Kitaigorodskii. J Geophys Res. 69:5191-203. http://dx.doi.org/10.1029/JZ069i024p05191.

Shen, W., Gurgel, K., Voulgaris, G., Schlick, T., & Stammer, D. 2012. Wind-speed inversion from HF radar first-order backscatter signal. Ocean Dynam. 62:105-21. http://dx.doi.org/10.1007/s10236-011-0465-9.

Stewart, R.H., & Barnum, J.R. 1975. Radio measurements of oceanic winds at long ranges: An evaluation. Radio Sci. 10:853-7. http://dx.doi.org/10.1029/RS010i010p00853.

Terray, E.A., Donelan, M.A., Agrawal, Y.C., Drennan, W.M., Kahma, K.K., Kitaigorodskii, S.A., … Williams, A.J., III. 1996. Estimates of kinetic energy dissipation under breaking waves. J Phys Oceanogr. 26:792-807. http://dx.doi.org/10.1175/1520-0485(1996)026<0792:EOKEDU>2.0.CO;2.

Wyatt, L., Ledgard, J., & Anderson, C.W. 1997. Maximum-likelihood estimation of the directional distribution of 0.53-Hz ocean waves. J Atmos Ocean Tech. 14:591-603. http://dx.doi.org/10.1175/1520-0426(1997)014<0591:MLEOTD>2.0.CO;2.

Wyatt, L.R. 2000. Limits to the inversion of HF radar backscatter for ocean wave measurement. J Atmos Ocean Tech. 17:1651-65. http://dx.doi.org/10.1175/1520-0426(2000)017<1651:LTTIOH>2.0.CO;2.

Wyatt, L.R., Green, J.J., Gurgel, K.-W.J., Nieto Borge, C., Reichert, K., Hessner, K., … Reistad, M. 2003. Validation and intercomparisons of wave measurements and models during the EuroROSE experiments. Coast Eng. 48:1-28. http://dx.doi.org/10.1016/S0378-3839(02)00157-6.

Wyatt, L.R., Green, J.J., & Middleditch, A. 2011. HF radar data quality requirements for wave measurement. Coast Eng. 58:327-36. http://dx.doi.org/10.1016/j.coastaleng.2010.11.005.